European Geothermal Congress 2013
Pisa, Italy, 3-7 June 2013

# Flow anisotropy in sheared fractures with self-affine surfaces

Martin Schoenball[1], Michael Selzer[2], Natalie Kühnle[1], Britta Nestler[2], Jean Schmittbuhl[3] and Thomas Kohl[1]

[1] Karlsruhe Institute of Technology, Institute of Applied Geosciences

[2] Karlsruhe Institute of Technology, Institute of Applied Materials

[3] University of Strasbourg, EOST

martin.schoenball@kit.edu

**Keywords:** fracture flow, modelling, EGS, cubic law.

## ABSTRACT

The hydraulic behavior of fractures is important for understanding geothermal reservoirs. Thus experimental and numerical analysis of fractures is important. The roughness of the surfaces of natural fractures has an effect on their permeability. Analytical methods fail to predict this effect in different scales. Here the hydraulic properties of rough fractures are investigated with numerical methods.

The fracture model consists of two identical self-affine surfaces, sheared element wise against each other. The heterogeneous aperture is represented by hydraulic conductivity in the numerical model. We use the finite element method in 2D for simulating the fluid flow through the fracture model. Fluid flow is forced with Dirichlet boundary conditions parallel and perpendicular to the shearing direction.

The calculated mean flow through all investigated fractures show an anisotropic behavior, dependent on the orientation of the pressure gradient. The flow parallel (perpendicular) to the shearing direction is increased (enhanced). The effect of channeling perpendicular to the direction is the reason for the anisotropy in fluid flow.

## 1. INTRODUCTION

Characterizing the hydraulic conductivities of rock masses is a key component during development and engineering of various underground installations like geothermal power plants, waste repositories or tunneling. The intrinsic permeability of intact rock is extremely low; however the rock mass usually contains a dense network of fractures with a relatively high hydraulic conductivity, which determine the hydraulic properties of the rock mass. To estimate hydraulic conductivities of fractures the cubic law for laminar fluid flow in a parallel plate model with constant aperture is commonly applied:

$$Q = \frac{a^2 g}{12 \nu} \frac{\Delta h}{\Delta L} B, \qquad [1]$$

where $Q$ is the fluid flow, $a$ the aperture, $g$ the gravitation acceleration, $\nu$ the kinetic viscosity, $\Delta h/\Delta L$ the hydraulic pressure gradient through the fracture and $B$ the width of the fracture.

However, the surface of natural fractures is rough, which strongly affects the hydraulic properties of fractures. First efforts to consider the roughness of fractures in fluid flow calculations were conducted experimentally by Lomize (1951), Louis (1967) and Witherspoon et al. (1980) who derived empirical relations describing the hydraulic behavior. These integrate fracture roughness into the cubic law, not considering scaling effects of fracture surface topography. Rock fractures consist of an upper and a lower fracture surface and an open fracture aperture in between. At some points both fracture surfaces touch, creating contact areas with zero conductivity. These contact areas and areas of low aperture limit fluid flow in the fracture which creates curved fluid flow paths and tortuosity which reduces hydraulic conductivity.

Most of the empirically derived laws were obtain from the study of laboratory scale samples and various testing methods on them. To extrapolate these findings to hectometric or kilometric scales of typical reservoirs the size effects must be taken into account (Murata et al., 2002) appropriately. In the course of development of fractal mathematics (Mandelbrot, 1985, Peitgen et al., 1988) the rough surfaces could be described as self-affine structures with a correlation between heights of asperities and their spatial distribution. Brown (1995, 1987) used this mathematical concept to describe surface roughness of fractures by a set of three parameters (fractal dimension, roughness, length scale). In addition, his approach makes it easy to create synthetic fracture surfaces for numerical studies (Brown et al., 1995, Glover et al., 1997).

To enhance fluid flow in a fractured rock mass, e.g. to create an enhanced geothermal system (EGS) (Genter et al., 2010), well bores in an intact rock mass are pressurized with fluid to reduce effective normal stresses of pre-existing fractures to enable shearing (Fjaer et al., 2008). Shearing usually enhances

hydraulic permeability as fractures experience opening by dilation (Barton et al., 1985, Willis-Richards et al., 1996, Chen et al., 2000). However, during shear small asperities of may be eroded creating additional contact areas that potentially reduce hydraulic conductivity (Zimmerman et al., 1992). Accompanying shearing motion of rock, hydraulic anisotropy develops which makes the rock more conductive parallel to the shearing direction and less conduction perpendicular to the shearing direction (Meheust and Schmittbuhl, 2001, Auradou et al., 2005, Yeo et al., 1998).

In this paper we quantitatively analyze hydraulic anisotropy introduced by shearing of synthetic fractures. Fractures are generated by shearing two identical fractal fracture surfaces incorporating dilation to obtain an aperture distribution. The geometrical properties of such created fractures are analyzed and their hydraulic properties investigated by numerical flow calculations using a finite element code. By studying anisotropy of a set of 1000 synthetic fractures we find that the magnitude and the scatter of anisotropy between the fractures increase with increasing amount of shearing. All sheared fractures, without exceptions, show a larger hydraulic permeability to flow perpendicular to the shearing direction than parallel to it.

## 2. 2D FRACTURE MODEL

We use the program SAFFT (Méheust &Schmittbuhl, 2001) to generate synthetic self-affine surfaces. The code creates normal distributed pseudo random numbers, which initially have no spatial correlation. By multiplying them with the spectral density function $G(k)$, a spatial correlation is introduced:

$$G(k) = Ck^{-\alpha}, \qquad [2]$$

where $k=2\pi/\lambda$ is the wave vector with the wavelength $\lambda$, $C$ is a constant and $\alpha$ is the slope of the so obtained logarithmic power spectrum (Brown, 1987). The slope $\alpha$ is related to the Hurst exponent $H$ by $H = (\alpha - 1)/2$ for fractal surfaces (Mandelbrot, 1983). The Hurst exponent is an index for the roughness of the surface. By applying the inverse Fourier transformation on the power spectrum a surface with spatially correlated values for the heights is obtained. As the code uses a fast Fourier transformation, surface sizes are restricted to $2^n$. In this study we use surface sizes of 128 × 128 to 512 × 512 elements. The Hurst exponent $H$, defining the fractal dimension $D$ of surface by $D = 3 - H$, is always set to $H$=0.8, being a universal value for granite (Boffa et al., 1998, Neuville et al., 2011), the typical reservoir rock for enhanced geothermal systems.

We base the scaling of the fractures on field measurements obtained from real granite by Schmittbuhl et al. (1993). Therefore for a typical fracture size a variation of the topography in the order of 30 mm is employed.

To generate a sheared fracture two identical generated self-affine surfaces are shifted by a number of elements. The vertical height of the upper surface is then adjusted such that both surfaces do not intersect but are in contact on at least one contact point. The difference between both surface heights is taken as the sheared fracture's aperture (Figure 1: Construction of aperture from identical lower and upper surfaces and a horizontal shearing by 20 elements with the assumption of a contact point.

). Although we do not take into account any material abrasion of small rock asperities or other mechanical interaction of the fracture surfaces we will use the term shearing for this process in the following.

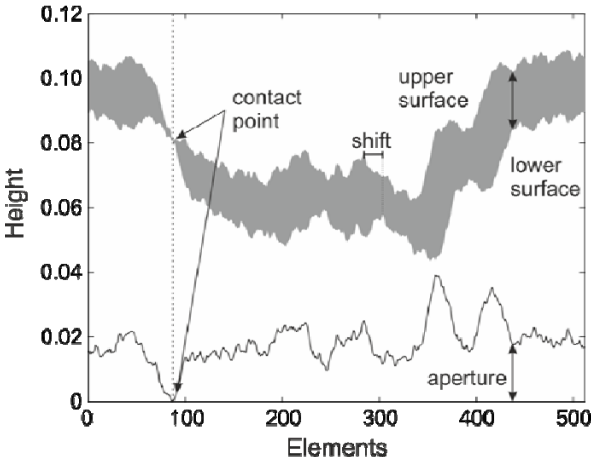


**Figure 1: Construction of aperture from identical lower and upper surfaces and a horizontal shearing by 20 elements with the assumption of a contact point.**

The arithmetic mean $\bar{a}$ and the standard deviation $\sigma$ of the aperture heights $a_i$ are calculated with every shearing step using the equations

$$\bar{a} = \frac{1}{n}\sum_{i=0}^{n} a_i \qquad [3]$$

and

$$\sigma = \sqrt{\frac{1}{n-1}\sum_{i=0}^{n}(a_i - \bar{a})^2}. \qquad [4]$$

Figure 2: Mean aperture (top) and standard deviation (bottom) of aperture as a function of the element-wise horizontal shear for four fractures of grid size 512 × 512 elements.

shows the mean aperture and the standard deviation as a function of the horizontal shear for four fractures with the grid size of 512 × 512 elements. Both, the mean and the standard deviation of the aperture, grow almost linearly with the shearing steps. This is in agreement with laboratory measurements of granite samples (Chen et al., 2000).

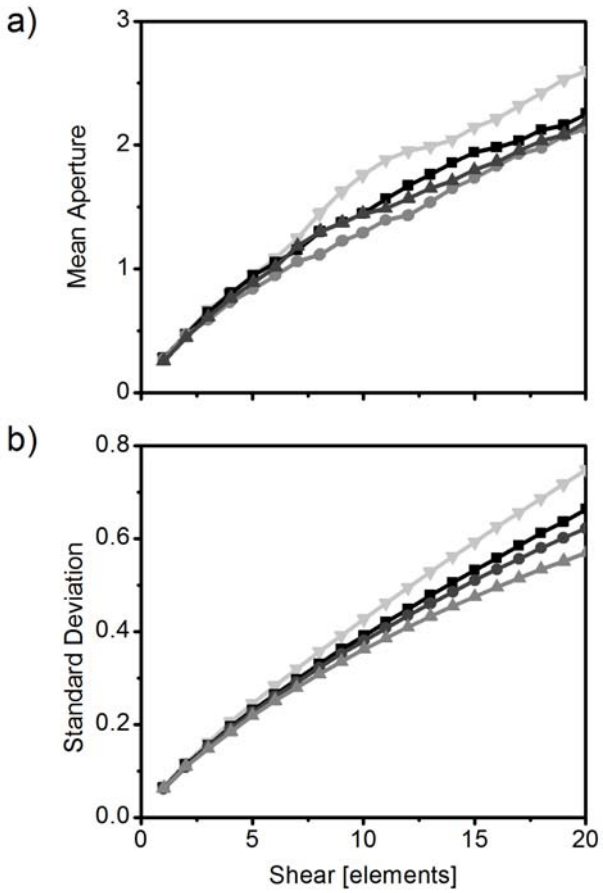


**Figure 2: Mean aperture (top) and standard deviation (bottom) of aperture as a function of the element-wise horizontal shear for four fractures of grid size 512 × 512 elements.**

## 3. NUMERICAL SIMULATIONS

For numerical simulations we use the finite element program FRACTure (Kohl & Hopkirk, 1995), which solves the partial differential equation describing pressure diffusion:

$$K \nabla^2 P = 0, \qquad [5]$$

where $K$ is the hydraulic conductivity and $P$ the pressure. The hydraulic conductivities $K_i$ for each element $i$ are calculated with the local aperture heights $a_i$ using the cubic law:

$$K_i = \frac{k_i}{\mu} = \frac{a_i^2}{12\mu} \qquad [6]$$

Here $k_i$ is the permeability and $\mu$ the dynamic viscosity. The numerical simulations were done using Dirichlet boundary conditions. The pressure at one border is set with $P = 1$ and at the opposed border with $P = 0$. At this stage simulations were run dimensionless, as we do not include non-linear flow behavior (turbulent flow, tortuosity, etc.) in the simulation of the hydraulic behavior of fractures. For each fracture we run two numerical simulations. First we set the boundary conditions parallel to the shearing direction and second perpendicular to the shearing direction.

In Figure 3 the positions of the Dirichlet boundary conditions and the evolving forced fluid flow $Q_{x1}$ and $Q_{x2}$ in the fracture are shown. $Q_{x1}$ is the flow perpendicular to the shearing direction and $Q_{x2}$ parallel to it.

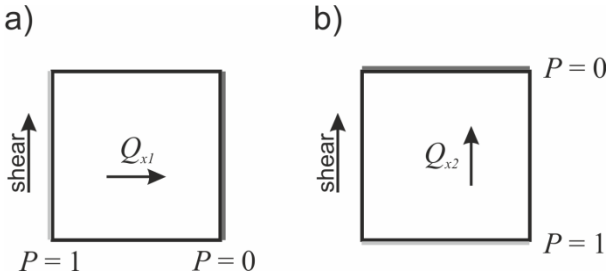


**Figure 3: Boundary conditions of the model a) for flow orthogonal to the shearing direction and b) for flow parallel to the shearing direction, which were run for each fracture.**

## 4. HYDRAULIC PRESSURE DISTRIBUTION IN THE FRACTURE

The numerical simulations with FRACTure result in a very heterogeneous pressure distribution in the fracture. Figure 4 c-d shows a pressure distribution with different flow directions in terms of isobars. Derived from this, different fluid velocities arise dependent on the boundary conditions. The fluid velocity $v_i$ of each element is the magnitude of the two fluid vector components in $x_1$- and in $x_2$-direction. The magnitude of the fluid velocity components are presented in Figure 4 e-f. The fluid velocities, where the flow is forced perpendicular to the shearing direction are higher than fluid velocities, where the flow is forced parallel to the shearing direction. Especially in regions with high permeability there are high fluid velocities by a pressure gradient perpendicular to the shearing direction (Figure 4 e-f). If you look at the same region, but with flow parallel to the shearing direction, the fluid velocities are much lower. The reason for this lies in the hydraulic barriers, where the pressure is highly reduced (Figure 4 c-d), so that after the barrier remains only low pressure gradients and the fluid velocity is low.

## 5. RESULTS

The results of the finite element simulation are used for calculating a mean flow through the fracture. The flow $Q_i$ for each element in the fracture is a multiplication of the modulus of the fluid velocities and the aperture height:

$$\frac{Q_i}{L} = |v_i| a_i \qquad [7]$$

The mean flow $\overline{Q}$ along the fracture width $L$ is the arithmetic mean of all elements:

$$\frac{\overline{Q}}{L} = \frac{1}{n} \sum_{i=0}^{n} \frac{Q_i}{L} \qquad [8]$$

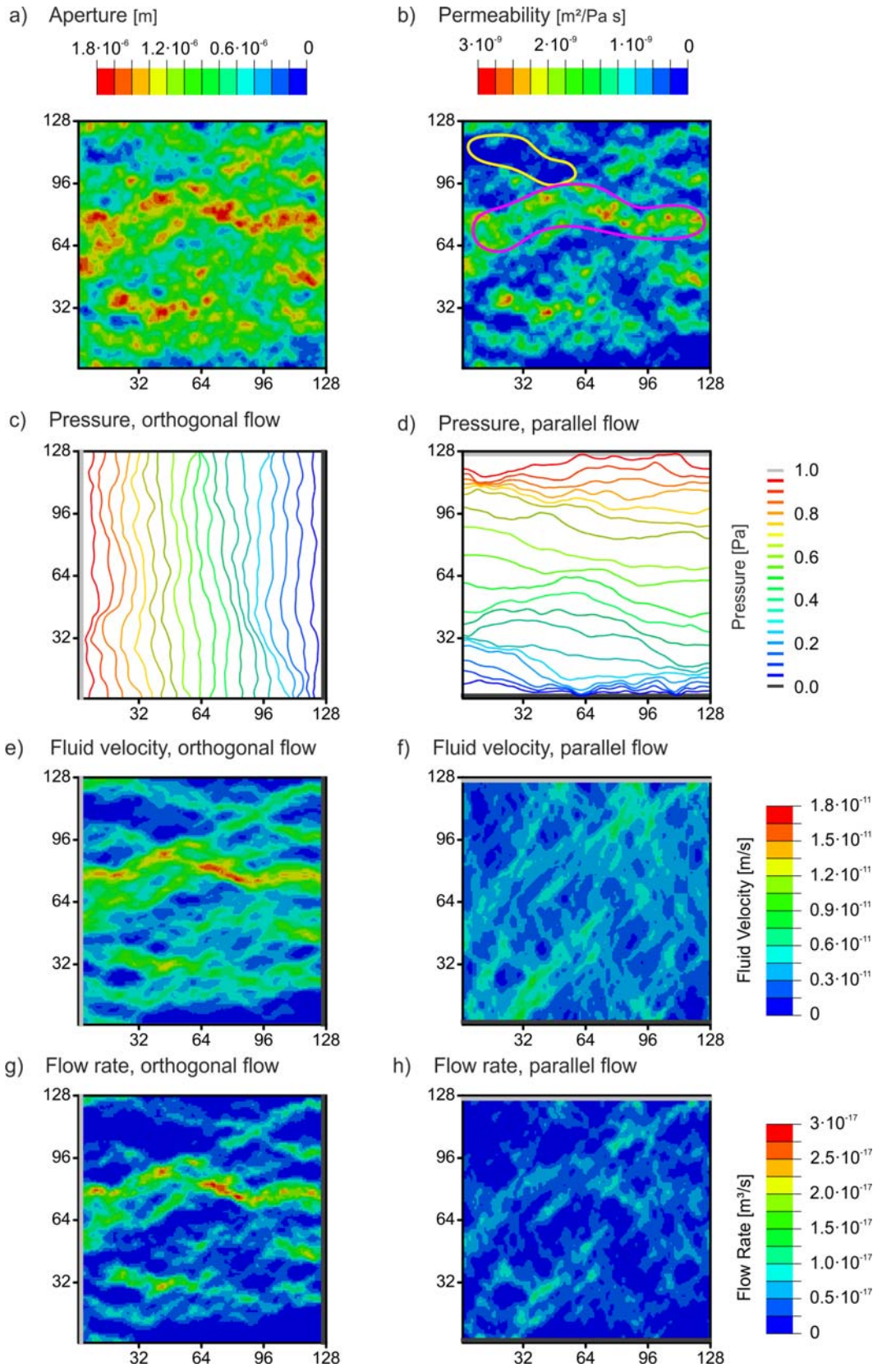


**Figure 4: Hydraulic properties of a fracture of 128 × 128 elements in size and sheared with displacement of 0.375 elements. (a) Aperture and (b) permeability with marks on a flow channel (magenta) and a hydraulic barrier (yellow). (c-d) show the pressure profile for the two flow simulation, (e-f) show the magnitude of fluid velocity and (g-h) show the fluid flow rate per element.**

The index *i* represents the element number and *n* the whole number of elements in the 2D fracture model.

According to the different position of Dirichlet boundary conditions (Figure 4) fluid flow is parallel to shearing direction of orthogonal to the shearing

direction. Interestingly, the hydraulic flux (Equation 9) is different for both model runs. The fracture gets hydraulically anisotropic through the shearing process. The flux parallel to shearing direction is less that orthogonal to the shearing direction (Figure 5). For reference we calculate the flux for the parallel plate model using the average geometric aperture and the cubic law. For every fracture the hydraulic flux of this parallel plate model is between the two fluxes (parallel and orthogonal) of the rough fractures. The hydraulic anisotropy is observed for each fracture analyzed but varies widely in a range of at least 6 % to 76 %. Exceptionally high magnitudes of anisotropy are results of local features, which arise from the fracture wall topography and the shearing. In the case of fracture 2 of size 128 × 128 are long hydraulic barrier (marking in Figure 4 b) of very small aperture and thus hydraulic conductivity is created by the shearing. This barrier hinders fluid flow orthogonal to the shearing direction.

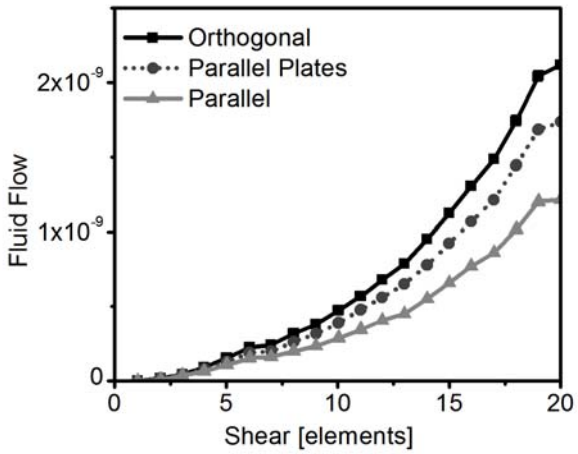


**Figure 5: Average flux per fracture width orthogonal to shearing direction (black), parallel to shearing (blue) and the parallel plate model (red) calculated from mean geometric aperture for reference. Fracture 2 of grid size 128 × 128 elements.**

The effect of shear induced anisotropy has already been observed numerically by Méheust & Schmittbuhl (2001) and numerically and experimentally by Auradou et al. (2005). Contrary to Auradou et al. (2005) we do not find increasing anisotropy with increasing shear for every single fracture. Instead for some fractures we see decreasing or roughly constant anisotropy, while for some others anisotropy increases considerably with increasing shear (Figure 6). The different response of the anisotropy characteristic to different magnitudes of shear is evidence for the importance of the actual fracture topography on the hydraulic properties. Furthermore, synthetic fractures of larger grid size show smaller variations of anisotropy among several fractures. For a larger number of discretized elements, extrema with small apertures are less important for the hydraulic behavior of the whole fracture system.

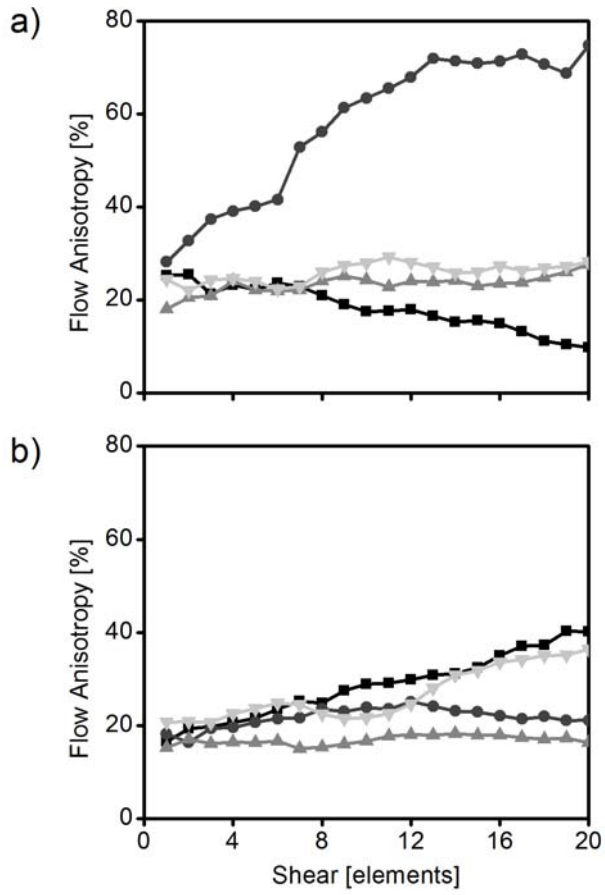


**Figure 6: Anisotropy of hydraulic flux [%] for grid size of 128 × 128 elements (left) and 512 × 512 elements (right).**

In the previous discussion several characteristics of the fractures and of the flow in these fractures were shown exemplarily for four synthetic fractures of 128 × 128 elements in size. Among these four fractures pronounced variations have been observed, leading to the need to analyze the fluid flow behavior in a statistically representative manner. Therefore we conducted an extensive study using a catalog of 1000 synthetic fractures of size 512 × 512 elements. For each fracture two simulations with the different boundary conditions relative to the shearing direction were run for each displacement step between 1 and 10 elements of shear. The result is a statistically representative study of the anisotropy behavior of fractures with different degrees of shear displacement (Figure 7). For small shear displacements we obtain a narrow distribution of anisotropy. With increasing shear displacement, the distribution widens considerably, and gets a positive skew, representing fractures with high values of hydraulic anisotropy. For low values of anisotropy the relative frequency is about constant or slightly decreasing for increasing shear displacement. The mean anisotropy value changes from 24% to 38% with increasing displacement. The overall change of anisotropy levels off, with very similar frequency distributions for displacements > 6 elements.

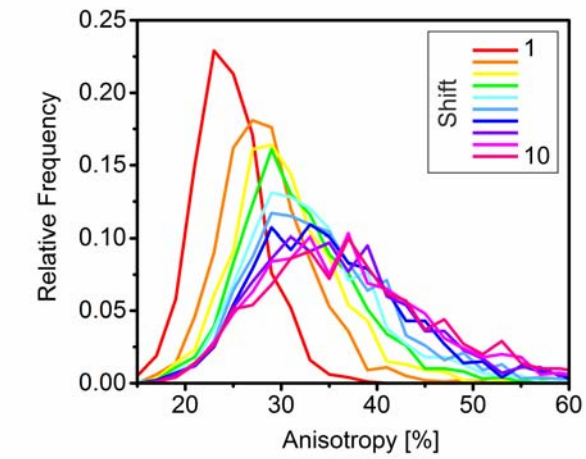


**Figure 7: Distribution of hydraulic anisotropy for different magnitudes of shear calculated from a set of 1000 fractures.**

## 6. CONCLUSIONS

We analyzed the hydraulic behavior of synthetically generated rough fractures. The 2D fracture model is made out of two identical self-affine fracture surfaces, which are sheared element-wise. Through the shearing process of the fracture surfaces the mean geometric aperture and its standard deviation are increasing continuously. The same effect can also be seen on the mean fluid flow. Dependent on the orientation of the boundary conditions different hydraulic flow is observed, each fracture shows hydraulic anisotropy but of a greatly varying degree dependent on the actual topography of the fracture. For every fracture we observe higher fluid flow orthogonal to the shearing direction and less fluid flow parallel to the shearing direction, when compared to the parallel plate model. Contrary to previous observations (Auradou et al., 2005) anisotropy may also decrease with increasing magnitudes of shear. No correlation between hydraulic anisotropy and mean aperture or standard deviation of aperture is observed. Instead, the hydraulic anisotropy originates from geometric barriers which form during the shearing process and limit fluid flow parallel to the shearing direction.

## REFERENCES

AURADOU, H., DRAZER, G., HULIN, J. P. & KOPLIK, J. (2005) Permeability anisotropy induced by the shear displacement of rough fracture walls. *Water Resour. Res.,* **41,** W09423.

BARTON, N., BANDIS, S. & BAKHTAR, K. (1985) Strength, Deformation and Conductivity Coupling of Rock Joints. *Int J Rock Mech Min,* **22,** 121-140.

BOFFA, J. M., ALLAIN, C. & HULIN, J. P. (1998) Experimental analysis of fracture rugosity in granular and compact rocks. *Eur. Phys. J.-Appl. Phys,* **2,** 281-289.

BROWN, S. R. (1987) A note on the description of surface roughness using fractal dimension. *Geophys. Res. Lett.,* **14,** 1095-1098.

BROWN, S. R. (1995) Simple Mathematical-Model of a Rough Fracture. *J Geophys Res-Sol Ea,* **100,** 5941-5952.

BROWN, S. R., STOCKMAN, H. W. & REEVES, S. J. (1995) APPLICABILITY OF THE REYNOLDS-EQUATION FOR MODELING FLUID-FLOW BETWEEN ROUGH SURFACES. *Geophysical Research Letters,* **22,** 2537-2540.

CHEN, Z., NARAYAN, S. P., YANG, Z. & RAHMAN, S. S. (2000) An experimental investigation of hydraulic behaviour of fractures and joints in granitic rock. *Int J Rock Mech Min,* **37,** 1061-1071.

FJAER, E., HOLT, R. M., HORSRUD, P., RAAEN, A. M. & RISNES, R. (2008) *Petroleum Related Rock Mechanics,* Elsevier.

GENTER, A., EVANS, K., CUENOT, N., FRITSCH, D. & SANJUAN, B. (2010) Contribution of the exploration of deep crystalline fractured reservoir of Soultz to the knowledge of enhanced geothermal systems (EGS). *Cr Geosci,* **342,** 502-516.

GLOVER, P. W. J., MATSUKI, K., HIKIMA, R. & HAYASHI, K. (1997) Fluid flow in fractally rough synthetic fractures. *Geophysical Research Letters,* **24,** 1803-1806.

KOHL, T. & HOPKIRK, R. J. (1995) FRACTURE - A SIMULATION CODE FOR FORCED FLUID-FLOW AND TRANSPORT IN FRACTURED, POROUS ROCK. *Geothermics,* **24,** 333-343.

LOMIZE, G. M. (1951) Strömung in klüftigen Gesteinen. *Gosenergoizdat, Moskau*.

LOUIS, C. (1967) Strömungsvorgänge in klüftigen Medien und ihre Wirkung auf die Standsicherheit von Bauwerken und Böschungen im Fels. In: *Institut für Bodenmechanik und Felsmechanik*. Universität Fridericiana Karlsruhe.

MANDELBROT, B. B. (Ed.) (1983) *The Fractal Geometry of Nature,* W.H.Freeman, New York.

MANDELBROT, B. B. (1985) Self-Affine Fractals and Fractal Dimension. *Phys Scripta,* **32,** 257.

MEHEUST, Y. & SCHMITTBUHL, J. (2001) Geometrical heterogeneities and permeability anisotropy of rough fractures. *J Geophys Res-Sol Ea,* **106,** 2089-2102.

MURATA, S., KYOTO UNIVERSITY; , H. MITSUISHI, J. N. O. C. & T. SAITO, K. U. (2002) Characterization of Fracture Permeability by Using a Fractal Model. *SPE Asia Pacific Oil and Gas Conference and Exhibition.*

NEUVILLE, A., TOUSSAINT, R. & SCHMITTBUHL, J. (2011) Fracture aperture reconstruction and determination of hydrological properties: a case study at Draix (French Alps). *Hydrological Processes,* p. 11.

PEITGEN, H. O., SAUPE, D. & BARNSLEY, M. F. (1988) *The science of fractal images,* Springer-Verlag New York.

SCHMITTBUHL, J., GENTIER, S. & ROUX, S. (1993) Field-Measurements of the Roughness of Fault Surfaces. *Geophysical Research Letters,* **20,** 639-641.

WILLIS-RICHARDS, J., WATANABE, K. & TAKAHASHI, H. (1996) Progress toward a stochastic rock mechanics model of engineered geothermal systems. *J Geophys Res-Sol Ea,* **101,** 17481-17496.

WITHERSPOON, P. A., WANG, J. S. Y., IWAI, K. & GALE, J. E. (1980) VALIDITY OF CUBIC LAW FOR FLUID-FLOW IN A DEFORMABLE ROCK FRACTURE. *Water Resources Research,* **16,** 1016-1024.

YEO, I. W., DE FREITAS, M. H. & ZIMMERMAN, R. W. (1998) Effect of shear displacement on the aperture and permeability of a rock fracture. *Int J Rock Mech Min,* **35,** 1051-1070.

ZIMMERMAN, R. W., CHEN, D.-W. & COOK, N. G. W. (1992) The effect of contact area on the permeability of fractures. *Journal of Hydrology,* **139,** 79-96.